crystals

MDPI

Article

On the Possibility of Using Secondary Alloys in the Production of Aluminum-Based Metal Matrix Composite

Lucia Lattanzi [1,*], Anders E. W. Jarfors [1] and Samuel A. Awe [2]

[1] Department of Materials and Manufacturing, School of Engineering, Jönköping University, Gjuterigatan 5, 553 18 Jönköping, Sweden; anders.jarfors@ju.se
[2] Automotive Components Floby AB, Aspenäsgatan 2, 521 21 Floby, Sweden; samuel.awe@acfloby.com
* Correspondence: lucia.lattanzi@ju.se

Abstract: Aluminum-based composites provide tribological performance and thermophysical properties that, combined with being lightweight, are suitable for their application in automotive brake discs. Aluminum alloys allow the use of secondary materials to produce composites, with the drawback of several elements, impurities, and oxides that can harm the mechanical and thermophysical properties. This preliminary study explored the mechanical and thermophysical performance of a composite material produced with a secondary matrix alloy. Overall, the results are promising, with a minimal decrease in mechanical and thermophysical properties despite clustered silicon carbide particles in the composite with the secondary matrix. The challenges in effectively dispersing carbides in the melt seem linked to aluminum oxides, and future microstructural investigations will aim to clarify this aspect.

Keywords: MMC; recycled alloys; aluminum; composite

check for updates

Citation: Lattanzi, L.; Jarfors, A.E.W.; Awe, S.A. On the Possibility of Using Secondary Alloys in the Production of Aluminum-Based Metal Matrix Composite. *Crystals* **2024**, *14*, 333. https://doi.org/10.3390/cryst14040333

Academic Editor: Tomasz Sadowski

Received: 19 March 2024
Revised: 26 March 2024
Accepted: 29 March 2024
Published: 31 March 2024

Copyright: © 2024 by the authors. Licensee MDPI, Basel, Switzerland. This article is an open access article distributed under the terms and conditions of the Creative Commons Attribution (CC BY) license (https://creativecommons.org/licenses/by/4.0/).

1. Introduction

Aluminum-based metal-matrix composites (MMCs) are valid candidates for substituting cast iron in the production of automobile brake discs [1,2]. These materials exhibit good tribological performances and suitable thermophysical properties in lightweight solutions. Two of the main challenges lie in the high-temperature mechanical properties and recyclability of the composite at the end-of-life of the product. Good high-temperature mechanical properties become less critical in regenerative braking in electric vehicles (EV) [3] compared to the requirements for mechanical braking in internal combustion engine (ICE) vehicles. Regenerative braking transfers less heat to the mechanical braking system, lowering the maximum operating temperature necessary for the application. Thus, aluminum-based MMCs are promising candidates for lightweight brake discs owing to their excellent wear resistance and satisfactory corrosion resistance, which are desirable for EV applications.

Regarding recyclability, Al allows the use of secondary alloys to produce MMCs. The drawback is that secondary aluminum alloys usually include several elements, impurities, and oxides that can harm the mechanical and thermophysical properties [4,5].

Despite the significant literature on aluminum-based MMCs reinforced with SiC particles [6–10], few recent studies have investigated the possibility of using secondary aluminum alloys to produce MMCs and recycle composite materials. Christy et al. [11–15] performed a series of studies to explore the possibility of using scrap aluminum alloy wheels (Al-4Si-3Mg-2Mn) to produce composites. Krishnan et al. [15] evaluated the materials' mechanical properties and wear resistance at room temperature. The authors observed a decrease in the tensile and compressive strengths of approximately 30% and 10%, respectively, compared to the composite produced with the primary Al-7Si-0.4Mg matrix alloy. The abrasive wear resistance of the composite, in terms of weight loss, remained constant and even improved with the coarsest grit of 20 when using the secondary alloy. These comparisons should be carefully considered because the matrix alloys differ, and the

reinforcement amount is not stated and evaluated in MMCs. Christy et al. [11] applied the Taguchi-Grey relational analysis method to optimize the squeeze casting parameters for the composite produced with scrap aluminum alloy wheels and alumina particles. The optimization was based on evaluating several microstructural and mechanical parameters, such as the porosity fraction, hardness, and tensile properties. Mourad et al. [14] continued with a similar procedure to produce hybrid composites reinforced with alumina, graphite, and silicon carbide (SiC) particles. The authors evaluated the mechanical properties and weldability of the composites and concluded that the material reinforced with 4% graphite was the most promising material for its mechanical strength. Thilak et al. [16] studied using a secondary Al-10Si-4Cu-1Fe alloy to produce composites reinforced with alumina particles. Bulei et al. [17] discussed the general benefits of using recycled aluminum alloys in aluminum-based composites, but specific results were not presented.

Studies on the possibility of recycling the composites at the product's end of life have been conducted in parallel with material development [18,19]. The idea is to have efficient recycling techniques when the current MMC products enter scrap streams. Sun et al. [20] worked on the production separation of the matrix alloy (A6061, Al-Mg-Si alloy) and the reinforcement particles (SiC) by supergravity technology. Among several process conditions, the authors found an optimum set of parameters to achieve recovery rates of 84% for the matrix alloy and 98% for SiC particles. Hirsch et al. [21] recently investigated a solid-state recycling route for aluminum matrix composites with a high-volume fraction of ceramic reinforcement. They concluded that the contamination level of the milled composite and consolidation method significantly influenced the properties of the recycled MMC.

The interest in the sustainability of composites is increasing steadily, and further investigation is needed when secondary aluminum alloys are included as the matrix. This study presents the preliminary results of the MaReAl research project, which aims to select the maximum amount of recycled alloy to produce automotive brake discs in aluminum-based MMCs. The scope of this study was to characterize Al-Si-based MMCs reinforced with 20 wt.% of SiC particles. The composites were produced by squeeze casting using a 100% secondary alloy for the matrix and were compared to the current solution developed for light brake discs. The thermal conductivity and mechanical properties at high temperatures were investigated because they are critical material properties for excellent-performing automotive brake discs [22].

2. Materials and Methods

The composite materials were produced by Automotive Components Floby AB (Floby, Sweden) using a squeeze casting technique. The matrix was an Al-10Si-Mg (EN AB 43000, equivalent to A360) alloy purchased from Stena Aluminium AB (Älmhult, Sweden), reinforced with 20 wt.% SiC particles. The amount of SiC particles is the same as SICAlight [23], the commercial aluminum-based composite available at Automotive Components Floby AB.

The SiC particles were purchased from Fiven ASA (Oslo, Norway) and were composed of cubic β-SiC and hexagonal/rhombic α-SiC structures, with an average particle size of 20 μm. The details of the casting procedure are described elsewhere [24].

The chemical compositions of the composites were measured using an optical emission spectrometer (Spectromaxx CCD LMXM3, Spectro Analytical Instruments), and the values in wt.% are presented in Table 1. The codename MMC_1 denotes the composite based on the primary matrix alloy, and MMC_2 denotes the composite with a secondary matrix alloy. The Si content includes the Si of the matrix alloy and carbides.

The iron (Fe)-based gray cast iron (GCI) typically used in brake-disc applications was also investigated for comparison. The weight percentages of the alloying elements were 3.7% carbon (C), 2.0% silicon (Si), 0.7% manganese (Mn), 0.05% phosphorous (P), 0.14% sulfur (S), 0.10% chromium (Cr), and 0.17% copper (Cu).

The iron (Fe)-based gray cast iron (GCI) typically used in brake-disc applications was also investigated for comparison. The weight percentages of the alloying elements were

3.7% carbon (C), 2.0% silicon (Si), 0.7% manganese (Mn), 0.05% phosphorous (P), 0.14% sulfur (S), 0.10% chromium (Cr), and 0.17% copper (Cu).

Table 1. The chemical composition [wt.%] of the MMCs measured by OES. The Si content includes the Si of the matrix alloy and carbides.

Element	MMC_1	MMC_2
Silicon (Si)	>24	>24
Iron (Fe)	0.22 ± 0.07	0.41 ± 0.01
Copper (Cu)	0.41 ± 0.06	0.71 ± 0.05
Manganese (Mn)	0.01 ± 0.001	0.34 ± 0.01
Magnesium (Mg)	0.41 ± 0.01	0.31 ± 0.09
Titanium (Ti)	0.08 ± 0.003	0.06 ± 0.002
Aluminum (Al)	balance	balance

The samples for material characterization were machined from the ingots produced via squeeze casting. The microstructure was evaluated using optical microscopy (DSX1000, Olympus, Tokyo, Japan), scanning electron microscopy, and transmission scanning electron microscopy (STEM) (Lyra3, Tescan, Brno, Czech Republic) coupled with energy-dispersive X-ray spectroscopy (Apollo, EDAX, Pleasanton, CA, USA). A thin lamella was machined on the same equipment using focused ion beam (FIB) milling with a gallium (Ga) source. The quantitative image analysis to evaluate the amount of clustered SiC particles and porosity was performed on the MIPAR software (Version 1) on five micrographs for each material, with the field of view covering the cross-section of the sample with a 10.5 mm diameter.

The thermophysical properties were measured in the 25–500 °C temperature range at a 10 K/min heating rate. Different techniques were used: the thermal diffusivity (α, [m/s^2]) was evaluated by laser flash analysis (LFA 427, Netzsch, Selb, Germany) in an argon (Ar) atmosphere; the coefficient of thermal expansion (CTE) was evaluated by dilatometry (DIL 402, Netzsch) in a helium (He) atmosphere; and the specific heat capacity (c_m, [J/kg*K]) was evaluated by differential scanning calorimetry (DSC 402, Netzsch) in an Ar atmosphere. The evolution of the density (ρ, [kg/m^3]) with temperature was calculated according to Equation (1) [25,26]:

$$\rho(T) = \rho_{RT}/(1 + CTE \times \Delta T)^3. \quad (1)$$

The composites' room temperature (RT) density of the composites was measured using the Archimedes principle. The thermal conductivity (λ, [W/m·K]) was calculated as the product of these three properties according to Equation (2) [27]:

$$\lambda(T) = \alpha(T) \times \rho(T) \times c_m(T), \quad (2)$$

The volumetric heat capacity (c_v, [J/m^3*K]) was calculated using Equation (3) [28]:

$$c_v(T) = \rho(T) \times c_m(T). \quad (3)$$

Tensile and compression tests were conducted on at least two cylindrical samples for each condition at room temperature and elevated temperatures (350, 420, and 470 °C) using a universal testing machine (Z100 Universal Testing Machine, Zwick Roell, Ulm, Germany). The tensile and compression specimens were fabricated from squeezed cast bars (Figure 1a). The squeezed cast bar was first sliced into four rectangular bars (Figure 1b) via waterjet cutting. After that, cylindrical bars test samples were produced from rectangular bars using conventional machining. The tensile samples for room-temperature testing had a gauge length of 30 mm and a gauge diameter of 6 mm (Figure 1c), and the tensile samples for high-temperature testing had a gauge length of 40 mm and a gauge diameter of 6 mm (Figure 1d). The tensile tests were conducted according to the ASTM E8 standard [29]. The compression samples had a diameter of 10 mm and an initial height of 15 mm (Figure 1e) and were fabricated using wire-cut electrical discharge machining (EDM). Compression tests were conducted according to the ASTM E9 standard [30].

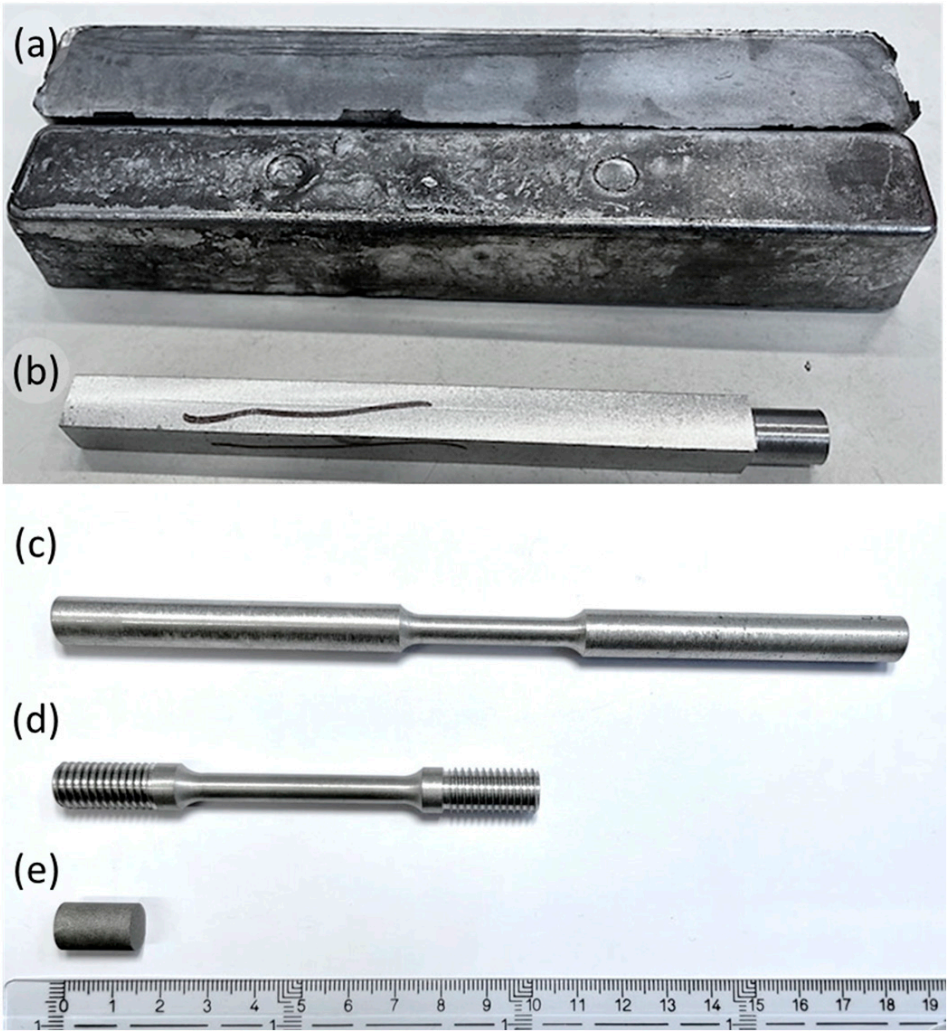


Figure 1. Sample production for mechanical testing: (**a**) squeeze casting ingots; (**b**) rectangular bars obtained by waterjet cutting; (**c**) tensile sample for room temperature testing; (**d**) tensile sample for high-temperature testing; (**e**) compression sample for testing at room temperature and high temperatures.

3. Results

This section presents the results of the experimental testing, starting with the microstructural characterization of the two composite materials. The thermophysical properties, mechanical characteristics, and wear performance were reported.

3.1. Microstructure

Figure 2 shows the characteristic macrostructures of these two materials. The MMC produced with the secondary alloy (Figure 2c) presented more clustered SiC particles than the material produced with the primary matrix (Figure 2a). In both materials, the microstructure of the matrix alloy was characterized by dendrites of primary aluminum (α-Al) and eutectic silicon particles. Polygonal SiC particles are recognized as dark features in the BSE images. At high magnification, it is possible to observe that the presence of porosity is often connected or close to the carbide clusters in MMC_2, as depicted in Figure 2d. In contrast, in MMC_1, the SiC particles were randomly dispersed in the matrix alloy (Figure 2b). Quantitative image analysis of SiC clusters larger than 0.04 mm^2 and porosity resulted in 1% and 0% area fractions for the MMC_1 material, respectively. The same evaluation resulted in a 3% area fraction of clusters larger than 0.04 mm^2 and a 0.3–1.2% area fraction of porosity.

Secondary aluminum alloys are prone to aluminum double oxide films, also called bifilms [31,32], which float in the melt. As shown in Figure 2a, the higher degree of clustering of SiC particles is probably related to the presence of oxide films that wrap the carbides and hinder their dispersion in the melt.

To investigate this aspect further, a thin lamella for STEM analysis was extracted from what looked like a closed oxide film, as depicted in Figure 3a, and studied using an optical microscope. The same region was identified in the SEM image, shown in Figure 3b (back-scattered electron SEM image), to extract a lamella transverse to the oxide film. The solid white line in Figure 3b represents the lamella orientation. The lamella in Figure 3c was roughly 200 nm thick, showing how the surface discontinuity was an opening in the subsurface region. The transmission EDS map analysis revealed the presence of Mg-based oxides around the opening. The gallium (Ga) element map confirmed that the built-up material linked to the milling steps did not affect the presence of such oxides, which lie in the aluminum regions surrounding the opening.

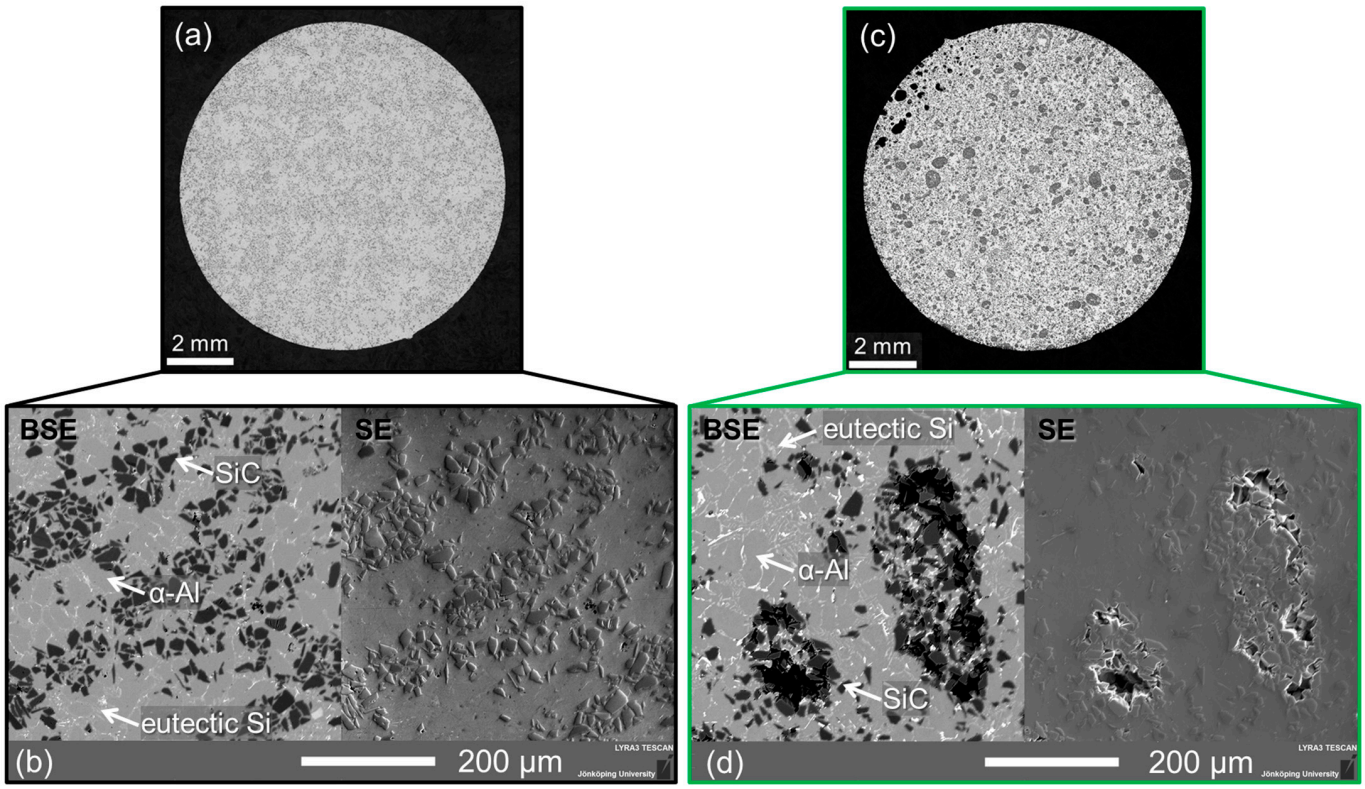


Figure 2. Composite MMC_1 (primary matrix alloy): (**a**) macrostructural overview (optical microscopy) and (**b**) SEM microstructure. Composite MMC_2 (secondary matrix alloy): (**c**) macrostructure overview (optical microscopy) and (**d**) SEM microstructure. The arrows in the SEM micrographs indicate the main microstructural features: primary aluminum (α-Al) dendrites, eutectic Si in the interdendritic regions, and SiC particles.

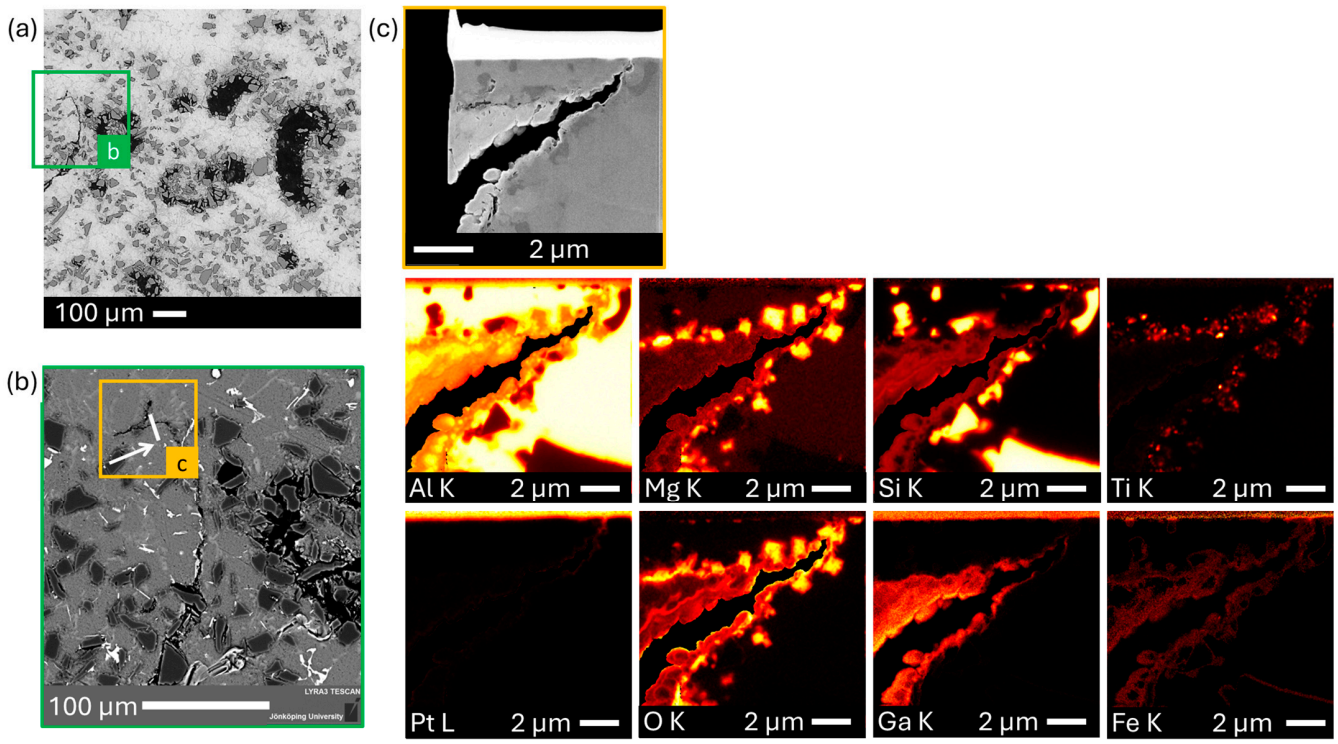


Figure 3. Investigation of the MMC_2 material: (**a**) optical micrograph and (**b**) backscattered electron SEM image of the green square in (**a**). The white arrow indicates the location where the lamella for STEM analysis was extracted, and the white solid line represents the orientation of the lamella; (**c**) the back-scattered electron micrograph of the lamella, extracted in the yellow square in (**b**), and the related EDS map.

3.2. Thermophysical Properties

Figure 4 summarizes the evolution of the thermophysical properties with temperature, comparing the composites with the primary and secondary matrix alloys. The density is presented in Figure 4a, and the porosity observed in Figure 2c in the MMC_2 composite affected the density of the material by 0.4%. As expected, the evolution of density with temperature, calculated using Equation (1), presented a constant decrease with increasing temperature.

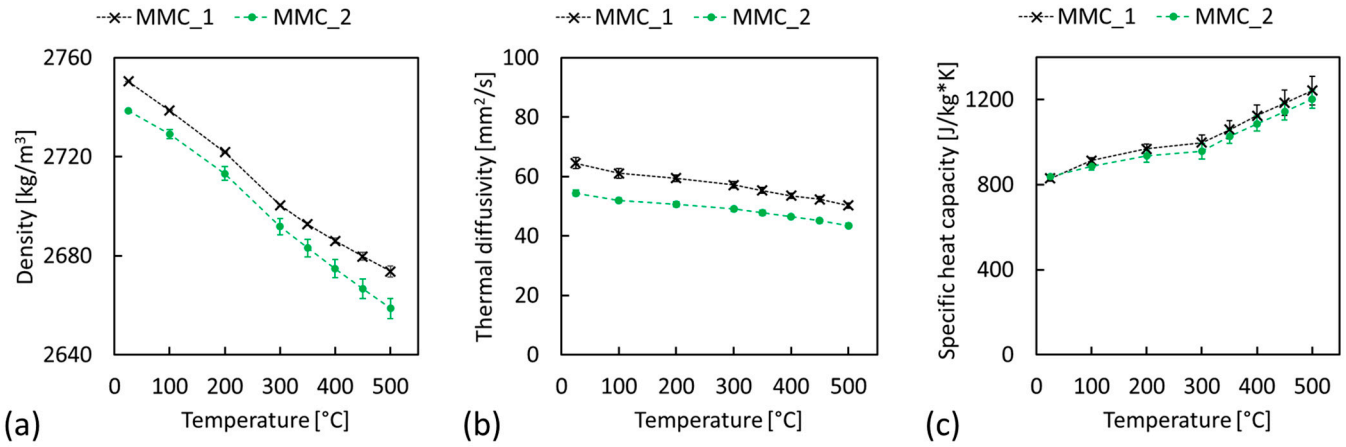


Figure 4. Evolution of thermophysical properties with temperature: (**a**) density [kg/m^3], (**b**) thermal diffusivity [mm^2/s], and (**c**) specific heat capacity [J/kg·K].

The evolution of the thermal diffusivity is presented in Figure 4b, and the MMC_2 composite presents 16% lower values than MMC_1 at room temperature. The difference remained almost constant as the temperature increased to 500 °C. Figure 4c shows the evolution of specific heat capacity with temperature. Here, the difference between the primary and secondary matrices is less evident than in the other properties. There was no significant difference at room temperature, and with increasing temperature, the MMC_2 material presented slightly lower values on average despite the overlapping error bars.

The thermal conductivity and volumetric heat capacity are presented in Figure 5a and Figure 5b, respectively, where GCI data are also presented for comparison with the traditional materials used for brake discs.

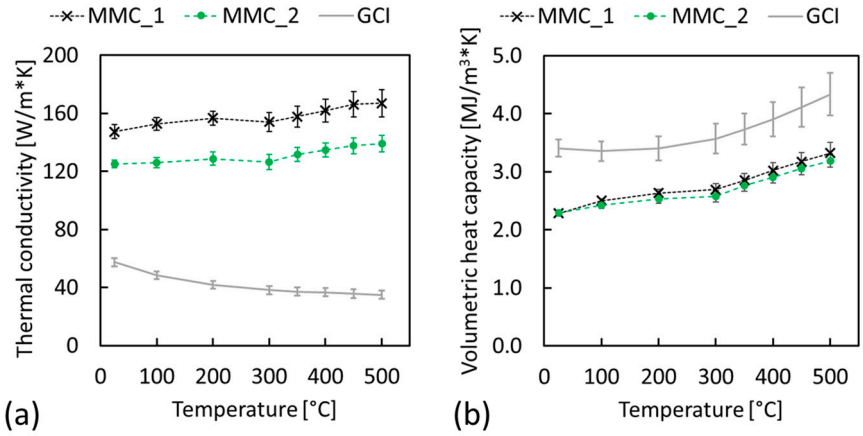


Figure 5. Evolution of thermophysical properties with temperature: (**a**) thermal conductivity [W/m·K]; (**b**) volumetric heat capacity [MJ/m^3·K].

The thermal conductivity in Figure 5a was calculated according to Equation (2), and the difference in the values between MMC_1 and MMC_2 reflects the differences observed in the properties of Figure 4. The presence of oxide-related porosities and clustered SiC particles affected the thermal conductivity of the MMC_2 composite, with a reduction of 15% from 147 to 125 W/m·K at room temperature. The thermal conductivity of MMC_2 remains lower than that of MMC_1 as the temperature increases from room temperature to 500 °C. Despite the decrease in the thermal conductivity linked to the secondary matrix alloy, the values were 117–140% higher than the GCI values.

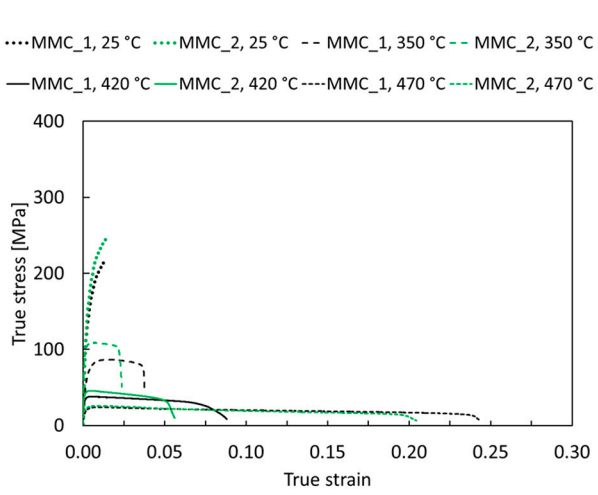
The volumetric heat capacity in Figure 5b was calculated using Equation (3). The difference between the composite materials over the tested temperature range is minimal. Compared to GCI, aluminum-based composites exhibit 25–40% lower values.

3.3. Mechanical Properties

Figure 6 summarizes the tensile test results at room and high temperatures. The elongation was limited for both materials at room temperature (approximately 1.3%) (Figure 6, dotted lines). The tensile strength was 10% higher for the composite with the secondary matrix alloy, and a similar difference was observed at 350 °C, although at lower strength values for both materials (Figure 6, dashed lines). The mechanical response of both materials was further affected by further increases in temperature to 420 °C (Figure 6, solid lines) and 470 °C (Figure 6, short-dashed lines), resulting in a significant decrease in tensile strength and an increase in elongation of up to 16–20%. The difference between the primary and secondary matrix alloys was not significant at these temperatures. The softening of the aluminum matrix at high temperatures seems to compensate for the negative impact of impurities that characterize the secondary alloy on the composite ductility.

Similar results were observed in the compression tests of the materials, as shown in Figure 7. At room temperature (Figure 7, dotted lines), MMC_2 presented a slightly higher average peak stress than MMC_1. Both materials presented a bump on the compression

curve after the peak stress corresponding to the cracking point of the outer material in the sample. This cracking event disappeared as the temperature increased to 350 °C (Figure 7, long dashed lines) due to the matrix's softening.



25 °C

Material	$R_{p0.2}$ [MPa]	R_m [MPa]
MMC_1	162 ± 11	212 ± 0
MMC_2	178 ± 4	236 ± 5

350 °C

Material	$R_{p0.2}$ [MPa]	R_m [MPa]
MMC_1	73 ± 1	86 ± 1
MMC_2	94 ± 11	102 ± 6

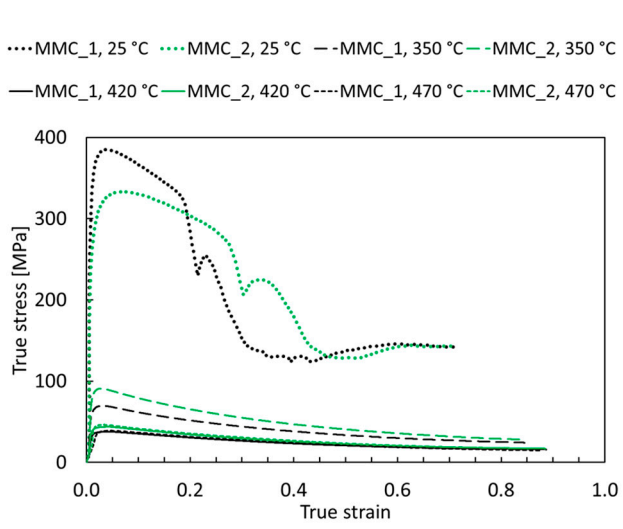
420 °C

Material	$R_{p0.2}$ [MPa]	R_m [MPa]
MMC_1	37 ± 1	38 ± 1
MMC_2	46 ± 1.5	47 ± 1

470 °C

Material	$R_{p0.2}$ [MPa]	R_m [MPa]
MMC_1	21 ± 1	24 ± 1
MMC_2	22 ± 2	23 ± 2

Figure 6. Tensile curves at different temperatures and related values of yield strength ($R_{p0\cdot2}$) and tensile strength (R_m) at room temperature, 25, 350, 420, and 470 °C.



25 °C

Material	Peak stress [MPa]
MMC_1	331 ± 75
MMC_2	336 ± 4

350 °C

Material	Peak stress [MPa]
MMC_1	77 ± 10
MMC_2	90 ± 1

420 °C

Material	Peak stress [MPa]
MMC_1	39 ± 1
MMC_2	45 ± 2

470 °C

Material	Peak stress [MPa]
MMC_1	39 ± 0.1
MMC_2	46 ± 1

Figure 7. Compression curves at different temperatures and related peak stress values were obtained at room temperature, 25 °C, 350 °C, 420 °C, and 470 °C.

On average, the MMC_2 material maintained a higher peak stress than the MMC_1 material as the temperature increased to 420 °C (Figure 7, solid lines) and 470 °C (Figure 7, short-dashed lines).

4. Discussion

Automotive brake discs require good mechanical performance at elevated temperatures and high thermal conductivity. Barton [33] suggested the "bucket and hole" analogy to evaluate the heat flow through a disc, and it is a helpful method to look for alternative materials for brake discs. One approach would be to rely on a material with a lower maximum operating temperature (MOT) than gray cast iron but with higher thermal conductivity. Aluminum-based composites satisfy this condition, and using a recycled matrix

alloy does not affect this property. Figure 8a shows that MMC_2 presents a reduced thermal conductivity compared with MMC_1, but the values are comparable to those of GCI. Owing to their high thermal conductivity values, aluminum composite brake rotors cool faster than the GCI equivalent because the heat generated during braking easily moves away from the friction surface to the surrounding components.

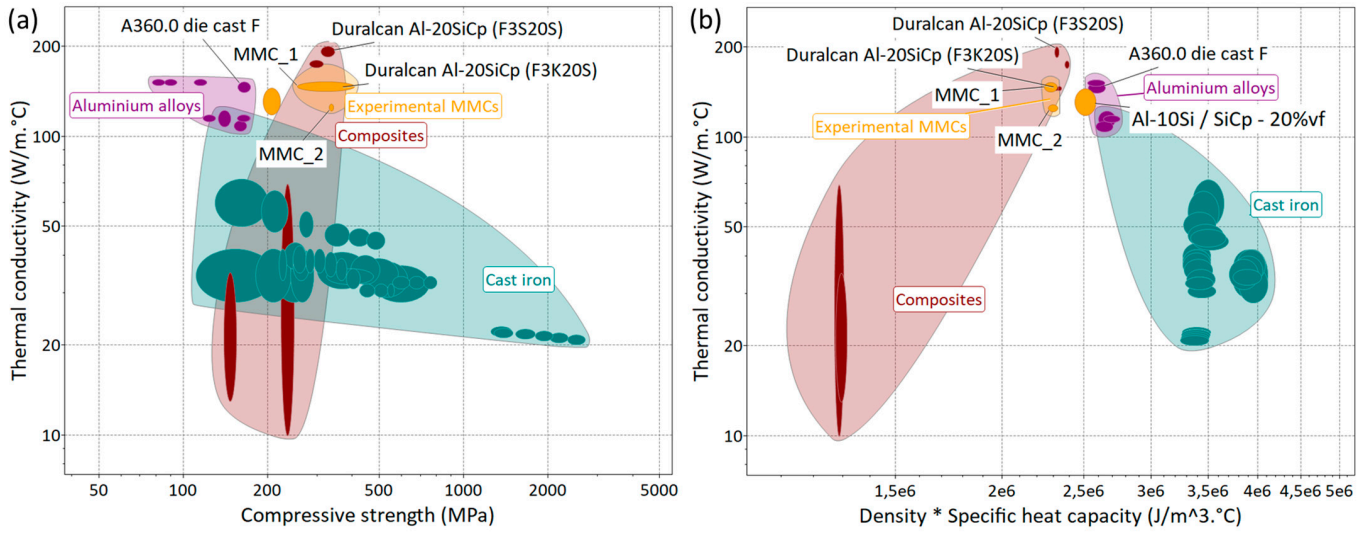


Figure 8. Plot of thermal conductivity and (**a**) compressive strength and (**b**) volumetric heat capacity = specific heat capacity × density. The axes of the ellipses represent the standard deviations of related material properties.

Figure 8b shows that the volumetric heat capacity on the horizontal axis is not affected by the secondary matrix alloy because the materials lie on the same vertical line. The volumetric heat capacity is particularly interesting for brake discs in EVs, where the regenerative braking system results in less heat transfer to the mechanical braking system than an ICE vehicle. Therefore, materials such as Al-MMCs with low volumetric heat capacity are suitable for braking rotors in EVs, where the volumetric heat capacity and, thus, the maximum operating temperature of the material can be lower than that of conventional brake rotors. An additional positive result is that the mechanical properties of the MMC_2 composite at high temperatures are not affected by the recycled matrix alloy, as shown in Figures 6 and 7.

The most significant benefit of using a secondary matrix alloy to produce a composite lies in the environmental properties of the material. The recycled material's CO_2 footprint (FP, expressed in kg/kg) and energy consumption (E, expressed in MJ/kg) were estimated using the Granta Selector software (Granta Selector 2023 R1, version 23.1.1) (Equation (4)).

$$\text{Recycled FP/E} = \left[\frac{100 - \text{R\%}}{100} \times \text{virgin FP/E}\right] + \left[\frac{\text{R\%}}{100} \times \text{recycling FP/E}\right] \quad (4)$$

In Equation (4), R% is the percentage of recycled material of a typical grade. The values for the CO_2 footprint and energy consumption of the Duralcan F3K20S material (Al-9Si/SiCp 20%) are listed in Table 2. The Duralcan F3K20S composite was most similar to the MMC_1 composite, and these data were used to estimate the values for MMC_1 and MMC_2. The resulting data are depicted in Figure 9a for direct comparison with commercially available composites of the Duralcan family.

The eco-audit example in Figure 9b,c is calculated for four brake discs on an electric family car that has been used for nine years, 365 days per year, and drives an average of 30 km per day. The evaluation was based on the usage in Europe. The GCI discs must be replaced thrice during the vehicle's life span; the use phase is the most energy-intensive for

the GCI discs, followed by the material production and manufacturing stages (Figure 9b). Similar evaluations were valid for the CO_2 footprint (Figure 9c).

Table 2. CO_2 footprint and energy usage values in the Granta Selector 2023 R1 Metals Plus database related to the Duralcan F3K20S material (Al-9Si/SiCp 20%).

Element	CO_2 Footprint [kg/kg]	Energy [MJ/kg]
Virgin material	11.9–13.1	169–187
Recycling	2.37–2.62	30.2–33.4

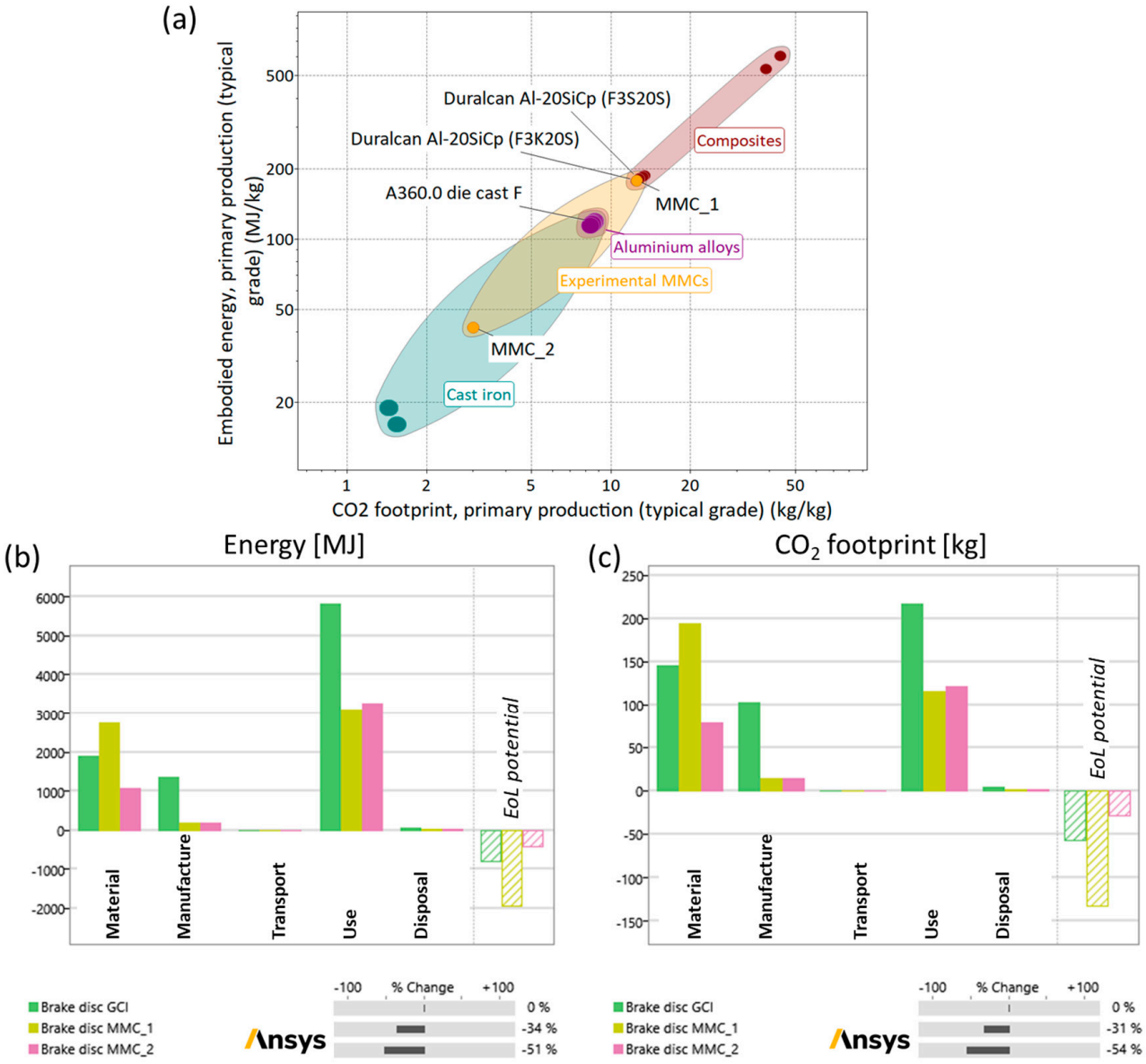


Figure 9. (**a**) Embodied energy v. CO_2 footprint for primary production of materials. Eco-audit in terms of (**b**) energy; (**c**) CO_2 footprint of the three materials of interest for automotive brake discs: grey cast iron (GCI), MMC_1, and MMC_2.

Brake discs in aluminum-based composites are more durable than GCI discs, and their lifetime is three times longer, according to AC Floby [23]. The energy-intensive phase for aluminum-based materials is the material production stage, which represents 45% of the total energy, and it is important to have a significant end-of-life credit of almost 70%. The

contribution of energy usage and the CO_2 footprint linked to material production can be significantly decreased by using recycled material for the matrix alloy to almost one-third of the values.

In summary, using aluminum composites reduced the total energy usage for brake discs by 34% and CO_2 emissions by 31% compared to GCI, which decreased both values by 51% and 54%, respectively. These values do not consider the end-of-life credit of the MMC_2 composite because its recyclability needs to be investigated for a comprehensive evaluation of energy usage and CO_2 emissions.

Future research will focus on component validation to describe how the properties tested at the laboratory scale characterize the performance of brake discs under different braking conditions. From a material point of view, the interaction between oxides and reinforcing carbides needs to be investigated further to understand the recycling possibilities of the composite itself.

5. Conclusions

The present study focuses on Al-Si-based MMCs reinforced with 20 wt.% SiC particles and produced with primary and secondary matrix alloys. The final application intended for this material is automotive brake discs. Preliminary tests indicated that the secondary matrix alloy did not significantly affect the thermal conductivity and mechanical properties at high temperatures. These promising results pave the way for comprehensive material characterization, including mechanical, wear and fatigue testing, on aluminum-based composites with different fractions of recycled matrix alloys to strengthen the results of the present study. The project aims to promote their development for other applications similar to automotive brake discs, which require good durability and mechanical resistance at elevated temperatures combined in a lightweight component.

Author Contributions: Conceptualization, L.L. and S.A.A.; methodology, L.L., A.E.W.J. and S.A.A.; validation, L.L., A.E.W.J. and S.A.A.; formal analysis, L.L.; investigation, L.L.; resources, A.E.W.J. and S.A.A.; data curation, L.L.; writing—original draft preparation, L.L.; writing—review and editing, A.E.W.J. and S.A.A.; visualization, L.L., A.E.W.J. and S.A.A.; project administration, L.L.; funding acquisition, L.L. All authors have read and agreed to the published version of the manuscript.

Funding: This research was funded by Vinnova through the Metalliska Material Strategic Innovation Program (grant number 2022-00828 MaReAl project).

Data Availability Statement: The data presented in this study are available upon request from the corresponding author. The data are not publicly available because of ongoing research.

Acknowledgments: Ansys is gratefully acknowledged for the Granta Selector software through the Research Partnership with Tekniska Högskolan i Jönköping. The authors gratefully acknowledge R. Westergård from Gränges Finspång AB, P. Jansson from Comptech i Skillingaryd AB, and T. Sjögren from RISE Borås as partners in the MaReAl project. N. Malo from ENSICAEN, Dharmateja Chalasani, and Johan Börjesson are acknowledged for supporting the experimental work. Some of these results were presented at the 5th International Conference on Light Materials, Science, and Technology (LightMAT 2023) in Trondheim.

Conflicts of Interest: The authors declare no conflict of interest.

References

1. Natarajan, N.; Vijayarangan, S.; Rajendran, I. Wear Behaviour of A356/25SiCp Aluminium Matrix Composites Sliding against Automobile Friction Material. *Wear* **2006**, *261*, 812–822. [CrossRef]
2. Awe, S.A.; Thomas, A. The Prospects of Lightweight SICAlight Discs in the Emerging Disc Brake Requirements. *Transport* **2021**, *13*, 14.
3. Gramstat, S. Technological Measures for Brake Wear Emission Reduction. In *Non-Exhaust Emissions*; Elsevier: Amsterdam, The Netherlands, 2018; pp. 205–227.
4. Ferraro, S.; Timelli, G. Influence of Sludge Particles on the Tensile Properties of Die-Cast Secondary Aluminum Alloys. *Metall. Mater. Trans. B* **2015**, *46*, 1022–1034. [CrossRef]

5. Sanchez, J.M.; Arribas, M.; Galarraga, H.; Garcia de Cortazar, M.; Ellero, M.; Girot, F. Effects of Mn Addittion, Cooling Rate and Holding Temperature on the Modification and Purification of Iron-Rich Compounds in AlSi10MnMg(Fe) Alloy. *Heliyon* **2023**, *9*, e13005. [CrossRef]
6. Lee, H.; Sohn, S.S.; Jeon, C.; Jo, I.; Lee, S.K.; Lee, S. Dynamic Compressive Deformation Behavior of SiC-Particulate-Reinforced A356 Al Alloy Matrix Composites Fabricated by Liquid Pressing Process. *Mater. Sci. Eng. A* **2017**, *680*, 368–377. [CrossRef]
7. Yang, X.; Barekar, N.S.; Ji, S.; Dhindaw, B.K.; Fan, Z. Influence of Reinforcing Particle Distribution on the Casting Characteristics of Al-SiCp Composites. *J. Mater. Process. Technol.* **2020**, *279*, 116580. [CrossRef]
8. Prakash, U.; Prasad, S.L.A.; Ravindra, H. V Study of Parametric Influence on Dry Sliding Wear of Al-SiCp MMC Using Taguchi Technique. *Mater. Today Proc.* **2015**, *2*, 1825–1832. [CrossRef]
9. An, Q.; Cong, X.; Shen, P.; Jiang, Q. Roles of Alloying Elements in Wetting of SiC by Al. *J. Alloys Compd.* **2019**, *784*, 1212–1220. [CrossRef]
10. Bushlya, V.; Lenrick, F.; Gutnichenko, O.; Petrusha, I.; Osipov, O.; Kristiansson, S.; Stahl, J.E. Performance and Wear Mechanisms of Novel Superhard Diamond and Boron Nitride Based Tools in Machining Al-SiCp Metal Matrix Composite. *Wear* **2017**, *376–377*, 152–164. [CrossRef]
11. Christy, J.V.; Arunachalam, R.; Mourad, A.H.I.; Krishnan, P.K.; Piya, S.; Al-Maharbi, M. Processing, Properties, and Microstructure of Recycled Aluminum Alloy Composites Produced Through an Optimized Stir and Squeeze Casting Processes. *J. Manuf. Process.* **2020**, *59*, 287–301. [CrossRef]
12. Christy, J.V.; Mourad, A.H.I. Friction Stir Welding of Hybrid Recycled Metal Matrix Composites. In Proceedings of the Pressure Vessels and Piping Division (Publication) PVP, Las Vegas, NV, USA, 17–22 July 2022; American Society of Mechanical Engineers: New York City, NY, USA; Volume 4-A. [CrossRef]
13. Christy, J.V.; Mourad, A.H.I.; Qudeiri, J.A. Tribological Analysis of Squeeze Stir Cast Recycled Aluminum MMC's. In Proceedings of the ASME 2021 Pressure Vessels & Piping Division (Publication) PVP, Virtual, 13–15 July 2021; American Society of Mechanical Engineers: New York City, NY, USA; p. 4. [CrossRef]
14. Mourad, A.H.I.; Christy, J.V.; Krishnan, P.K.; Mozumder, M.S. Production of Novel Recycled Hybrid Metal Matrix Composites Using Optimized Stir Squeeze Casting Technique. *J. Manuf. Process.* **2023**, *88*, 45–58. [CrossRef]
15. Krishnan, P.K.; Christy, J.V.; Arunachalam, R.; Mourad, A.-H.I.; Muraliraja, R.; Al-Maharbi, M.; Murali, V.; Chandra, M.M. Production of Aluminum Alloy-Based Metal Matrix Composites Using Scrap Aluminum Alloy and Waste Materials: Influence on Microstructure and Mechanical Properties. *J. Alloys Compd.* **2019**, *784*, 1047–1061. [CrossRef]
16. Thilak, R.; Rajan, K.; Ramesh, S.; Boppana, S.B.; Krishnan, P.K. Sustainable Development on Production and Characterization of Metal Matrix Composites Using Stir Casting. *J. Phys. Commun.* **2023**, *7*, 065002. [CrossRef]
17. Bulei, C.; Kiss, I.; Alexa, V. Development of Metal Matrix Composites Using Recycled Secondary Raw Materials from Aluminium Wastes. *Mater. Today Proc.* **2021**, *45*, 4143–4149. [CrossRef]
18. Skrobian, M.; Krahulec, J.; Krivan, P. Recycling of carbon containing aluminum matrix composites via their remelting. *Acta Metall. Slovaca* **2014**, *20*, 405–409. [CrossRef]
19. Mandal, D.; Viswanathan, S. Effect of Re-Melting on Particle Distribution and Interface Formation in SiC Reinforced 2124Al Matrix Composite. *Mater. Charact.* **2013**, *86*, 21–27. [CrossRef]
20. Sun, N.; Wang, Z.; Guo, L.; Wang, L.; Guo, Z. Efficient Separation of Reinforcements and Matrix Alloy from Aluminum Matrix Composites by Supergravity Technology. *J. Alloys Compd.* **2020**, *843*, 155814. [CrossRef]
21. Hirsch, S.J.; Grund, T.; Lampke, T. Towards Closed-Loop Recycling of Ceramic Particle-Reinforced Aluminium Alloys: Comparative Study of Resistance-Heating Sintered Primary and Solid-State Recycled Secondary SiCp/AlSi7Mg Composites. *Crystals* **2023**, *13*, 830. [CrossRef]
22. Thomas, A.; Zervos, N.; Ekelund, A.; Awe, S.A. Simulation Study on the Thermomechanical Behaviour of Al-MMC Automotive Brake Discs. *Eurobrake* **2019**, *2019*, 1–12.
23. SiCAlight—AC Floby. Available online: https://www.sicalight.com/ (accessed on 1 March 2024).
24. Lattanzi, L.; Etienne, A.; Li, Z.; Manjunath, T.; Nixon, N.; Jarfors, A.E.W.; Awe, S.A. The Influence of Ni and Zr Additions on the Hot Compression Properties of Al-SiCp Composites. *J. Alloys Compd.* **2022**, *905*, 164160. [CrossRef]
25. Density—NETZSCH Analyzing & Testing. Available online: https://analyzing-testing.netzsch.com/en/training-know-how/glossary/density (accessed on 14 December 2023).
26. Coefficient of Linear Thermal Expansion (CLTE/CTE)—NETZSCH Analyzing & Testing. Available online: https://analyzing-testing.netzsch.com/en/training-know-how/glossary/coefficient-of-linear-thermal-expansion-clte-cte (accessed on 14 December 2023).
27. Thermal Conductivity—NETZSCH Analyzing & Testing. Available online: https://analyzing-testing.netzsch.com/en/training-know-how/glossary/thermal-conductivity (accessed on 14 December 2023).
28. Specific Heat Capacity (Cp)—NETZSCH Analyzing & Testing. Available online: https://analyzing-testing.netzsch.com/en/training-know-how/glossary/specific-heat-capacity-cp (accessed on 14 December 2023).
29. E8/E8M Standard Test Methods for Tension Testing of Metallic Materials. Available online: https://www.astm.org/e0008_e0008m-22.html (accessed on 26 March 2024).
30. E9 Standard Test Methods of Compression Testing of Metallic Materials at Room Temperature. Available online: https://www.astm.org/e0009-09.html (accessed on 26 March 2024).

31. Gyarmati, G.; Fegyverneki, G.; Mende, T.; Tokár, M. Characterization of the Double Oxide Film Content of Liquid Aluminum Alloys by Computed Tomography. *Mater. Charact.* **2019**, *157*, 109925. [CrossRef]
32. Eisaabadi, B.G.; Davami, P.; Kim, S.K.; Tiryakioğlu, M. The Effect of Melt Quality and Filtering on the Weibull Distributions of Tensile Properties in Al–7%Si–Mg Alloy Castings. *Mater. Sci. Eng. A* **2013**, *579*, 64–70. [CrossRef]
33. Barton, D.C. Composite Materials for Automotive Braking Systems. In *Advanced Composite Materials for Automotive Applications*; Wiley: Hoboken, NY, USA, 2013; pp. 389–403.

Disclaimer/Publisher's Note: The statements, opinions and data contained in all publications are solely those of the individual author(s) and contributor(s) and not of MDPI and/or the editor(s). MDPI and/or the editor(s) disclaim responsibility for any injury to people or property resulting from any ideas, methods, instructions or products referred to in the content.